

A Comptonized Fireball Bubble: Physical Origin of Magnetar Giant Flares

ZHAO JOSEPH ZHANG (张钊)^{1,2} BIN-BIN ZHANG^{1,2} AND YAN-ZHI MENG^{1,2}

¹*School of Astronomy and Space Science, Nanjing University, Nanjing 210023, China*

²*Key Laboratory of Modern Astronomy and Astrophysics (Nanjing University), Ministry of Education, China*

ABSTRACT

Magnetar Giant Flares (MGFs) have been long proposed to contribute at least a sub-sample of the observed short Gamma-ray Bursts (GRBs). The recent discovery of the short GRB 200415A in the nearby galaxy NGC 253 established a textbook-version connection between these two phenomena. Unlike previous observations of the Galactic MGFs, the unsaturated instrument spectra of GRB 200415A provide for the first time an opportunity to test the theoretical models with the observed γ -ray photons. This paper proposed a new readily fit-able model for the MGFs, which invokes an expanding fireball Comptonized by the relativistic magnetar wind at photosphere radius. In this model, a large amount of energy is released from the magnetar crust due to the magnetic reconnection or the starquakes of the star surface and is injected into confined field lines, forming a trapped fireball bubble. After breaking through the shackles and expanding to the photospheric radius, the thermal photons of the fireball are eventually Comptonized by the relativistic e^\pm pairs in the magnetar wind region, which produces additional higher-energy gamma-ray emission. The model predicts a modified thermal-like spectrum characterized by a low-energy component in the Rayleigh-Jeans regime, a smooth component affected by coherent Compton scattering in the intermediate energy range, and a high-energy tail due to the inverse Compton process. By performing a Monte-Carlo fit to the observational spectra of GRB 200415A, we found that the observation of the burst is entirely consistent with our model predictions.

Keywords: Gamma-ray bursts; Gamma-ray transient sources; Magnetars, Giant flares

1. INTRODUCTION

Magnetars (Mereghetti et al. 2015; Kaspi & Beloborodov 2017) belong to a particular type of neutron stars carrying ultra-strong magnetic field typically in the range of $B \sim 10^{14}\text{-}10^{15}$ G (Duncan & Thompson 1992), much higher than the critical magnetic field, $B_Q = 4.4 \times 10^{13}$ G, above which the nonrelativistic Landau energy becomes comparable to the electron rest energy (Thompson & Duncan 1995). Observationally, magnetars are registered as two classes: the Anomalous X-ray Pulsars (AXPs) and the Soft Gamma-ray Repeaters (SGRs). SGRs have recently aroused increasing research interest due to their associations with Fast Radio Bursts (FRBs; Israel et al. 2016; Metzger et al. 2019; Katz 2020; Lin et al. 2020; Zhang 2020) and Gamma-ray Bursts (GRBs; Hurley et al. 1999; Yang et al. 2020; Roberts et al. 2021; Svinkin et al. 2021). In particular,

the magnetar giant flares (hereafter, MGFs) from the SGRs (Mazets et al. 1979a,b) have been long considered to be a subclass of short GRBs (Laros et al. 1986; Atteia et al. 1987).

The first magnetar giant flare (GRB 790305B) was observed from SGR 0526-66 (Golenetskii et al. 1984), which is located in the star-forming Dorado region in the Large Magellanic Cloud (LMC). Since then, two more Galactic MGF events have been confirmed, namely, the MGF of SGR 1900+14 on 1998 August 27 (Feroci et al. 2002) and the MGF of SGR 1806-20 on 2004 December 27 (Yamazaki et al. 2006). Located within a few \sim kpc, those events, although having provided enriched data in studying their temporal features (including the short abrupt rise, the quasi-exponential decay, the subsequent pulsating tail; Hurley et al. 1999; and the quasi-periodic oscillations; Israel et al. 2005; Strohmayer & Watts 2005) of the MGFs, are all observed saturated by the γ -ray detectors due to their overwhelmingly large numbers of photons. Thus, studying the accurate spectral data of MGF has been infeasible until the extra-

galactic MGF-originated event, GRB 200415A, was observed.

GRB 200415A is an apparent short gamma-ray burst discovered in the nearby Sculptor galaxy (NGC 253), which is located about 3.5 Mpc away (Bissaldi et al. 2020), much further than those in the previous MGF sample. A comprehensive analysis performed by Yang et al. (2020) suggests the burst is a significant outlier of both the Type I and Type II GRBs, but otherwise entirely consistent with being an MGF event in terms of the temporal and spectral features. Thanks to its significant distance outside the Milky Way, the bright GRB 200415A is not subject to instrumental saturation and provides an ideal case to study the photon behaviors of the MGFs. A spectral fit using some empirical functions suggested that the burst is dominated by thermal-like emissions (Yang et al. 2020), likely originates from an expanding fireball outside the magnetar surface and may be Doppler-boosted by the relativistic wind (Roberts et al. 2021).

Nevertheless, as a rare and most powerful type of SGR activity, MGFs' physical origin, trigger mechanism, and radiation process are still not fully unveiled. A trigger of an MGF can be caused either internally (e.g., large-scale star crust fracturing caused by the shear forces against the motion of the magnetic footpoints; neutral point reconnection due to the torsional of the twisted interior magnetic field; Parker 1983a,b; Thompson & Duncan 1995) or externally (e.g., interchange instability and/or magnetic reconnection; Moffatt 1985; Thompson & Duncan 2001). On the other hand, the radiation process models of MGFs are relatively less diverse. Thompson & Duncan (1995) proposed a “trapped fireball” model to explain the March 5th event on SGR 0526-66. The model introduces an initially expanding fireball to explain the first sharp spike of the MGF event. The fireball is eventually trapped by optically thick pair plasma in the stellar magnetosphere, producing repeated pulsations. In addition, Thompson & Duncan (1995) suggested that a relativistic wind driven by the pressure of the electron-position pair (e^\pm hereafter) plasma from the NS surface, which can also release a fraction of the star's energy. The prediction of the E_p -flux correlation of such a model was claimed to be consistent with the observation of GRB 200415A (Roberts et al. 2021). Although these studies may shed light on the origin and radiation mechanisms of the MGFs, a detailed first-principle calculation of such a scenario and its validation through a direct fit to the observed spectra is still missing to date.

Motivated by the previous studies, in this *Letter*, we studied in detail how the fireball expands from the NS surface and penetrates the area of the magnetar

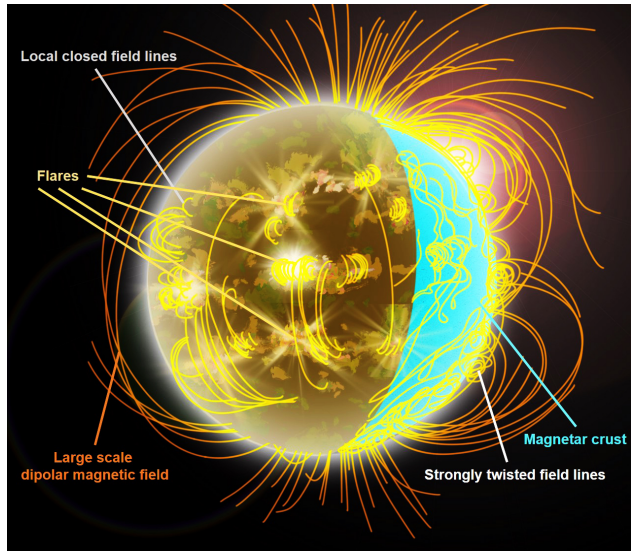


Figure 1. An illustration of the magnetic topology of the magnetar in our model.

wind. Our finding suggests that the fireball is eventually Comptonized by the dense e^\pm pair plasma at a much larger radius and produces a multi-component thermal-like radiation spectrum. Moreover, we directly compare this model with the spectral data of GRB 200415A. This *Letter* is organized as follows. We describe the physical picture of our model in §2. In §3, we formulated the radiation mechanism for the calculation of the specific flux and fit our model to the spectral data, constraining some physical parameters. A brief summary is presented in §4.

2. THE PHYSICAL PICTURE

Our model requires a magnetar characterized by a large-scale dipolar magnetic field with some small-scale and axisymmetric magnetic topology (Gourgouliatos et al. 2016). The small-scale field can be caused by internal motions such as the hall drift of the crustal magnetic field. As illustrated in Figure 1, the local small-scale magnetic field lines will be strongly wound up so that the toroidal component is greater than the poloidal dipole strength. Therefore, the local magnetic field may be an order of magnitude higher than that of the large-scale dipolar field, which can exceed $10^{16}G$. Under such an assumption, the physical picture of our model can be outlined in the following steps:

1. The occurrence of the small-scale magnetic instability. The Hall drift of the interior field lines and the activity of the NS crust can make the local external field become extremely unstable, causing strong magnetic reconnection.

2. The formation of the trapped fireball. Near the NS surface, an enormous amount of energy carried by photons is instantly released via the small-scale magnetic reconnection and interchange instability, and numerous e^\pm pairs escaped from the NS due to the fracturing of the crust. These photons and pairs, coupling with each other, are injected into the magnetosphere. A fraction of the energy of the photon-rich pair plasma is confined by the closed magnetic field lines and forms a trapped fireball as shown in figure 2.

Within the trapped fireball, the energy is gradually dissipated via thermal radiation with a timescale of up to hundreds of seconds. A pulsating tail is expected within such a long timescale due to the continuous local quasi-periodic activities of the magnetar. The total energy carried by the pulsating tail is roughly estimated as $E_{\text{tail}} \sim 10^{44}$ ergs in the previous three MGFs (Mereghetti 2008). To confine this amount of energy in the closed field lines, the pressure at the outer boundary of the field loop is required to satisfy (Yang & Zhang 2015)

$$\frac{B_{R_s+l_0}^2}{8\pi} \gtrsim \frac{E_{\text{tail}}}{3l_0^3}, \quad (1)$$

where R_s is the surface radius of the magnetar, and l_0 is the scale of the trapped fireball which in this case is smaller than R_s , i.e., $l_0 < R_s$ (c.f., Boggs et al. 2007). B_r is defined by $B_r = B_*(r/R_s)^{-3}$ for a dipolar field at radius of r , where B_* is the characteristic surface magnetic field of the neutron star.

Observationally, the size of the fireball can be estimated by

$$l_0 \sim \left(\frac{L_{\text{tail}}}{2\pi c a T_{\text{tail}}^4} \right)^{1/2} \sim 10^5 \text{ cm} \left(\frac{L_{\text{tail}}}{5 \times 10^{43} \text{ erg s}^{-1}} \right)^{1/2} \times \left(\frac{k T_{\text{tail}}}{70 \text{ keV}} \right)^{-2}, \quad (2)$$

where a is the radiation constant, and T_{tail} is the thermal equilibrium temperature which can be estimated by the cutoff energy T_{cut} . The characteristic values of $L_{\text{tail}} \sim 5 \times 10^{43} \text{ erg s}^{-1}$ and $k T_{\text{tail}} = 70 \text{ keV}$ in Eq. (2) are comparable to those observed in SGR 1806-20.

3. The formation of the magnetar wind. Due to the significant pressure of the photon-pair plasma,

numerous e^\pm is driven from the magnetosphere. These pairs, after being accelerated by the gap potential difference, produce the high-energy curvature radiation, which is influenced by the magnetic field, in turn, can be converted into secondary e^\pm pairs. As a result, the e^\pm pairs increase rapidly in number and move along the field lines, forming a relativistic wind (Figure 2). The magnetar wind will supply a high number density of charged particles (i.e., electrons and positrons) which can be calculated (Kumar & Bošnjak 2020) as a function of the magnetic field, B_* , the rotation period, P , and the distance to the center of the magnetar, R , as

$$n_\pm = \frac{\mathcal{M} \mathbf{B}_0 \cdot \Omega_*}{2\pi qc} \approx 2 \times 10^{25} \text{ cm}^{-3} \left(\frac{\mathcal{M}}{10^9} \right) \left(\frac{P}{1 \text{ s}} \right)^{-1} \left(\frac{B_*}{5 \times 10^{16} \text{ G}} \right) \times \left(\frac{R}{R_s} \right)^{-3}, \quad (3)$$

where \mathcal{M} is the multiplicity parameter defined as the ratio of maximum Lorentz factor of primary electrons and secondary e^\pm pairs, which can be estimated up to $\sim 10^9$ for a magnetar (Ruderman & Sutherland 1975).

4. The expanding of the fireball. The fireball will break through the shackles of the field lines and expand along the magnetic tube when the radiation pressure of the fireball is stronger than the magnetic pressure. The local magnetic field lines become open during the expansion (figure 2). For a dipolar field, the bulk Lorentz factor and comoving temperature are determined by the local acceleration as well as the size of expanding fireball, l :

$$\Gamma = (l/l_0)^{3/2}, \quad T = T_{\text{ini}}(l/l_0)^{-3/2}, \quad (4)$$

where T_{ini} and l_0 are the initial temperature and radius of the trapped fireball, respectively. We set $k T_{\text{ini}} = 844 \text{ keV}$, which is obtained from observations of the GRB 200415A (Yang et al. 2020).

5. The interaction between the expanding fireball and the wind. The fireball expands relativistically and penetrates to the wind zone within the magnetosphere. The photosphere radiation is generally considered to be thermal; therefore, blackbody radiation is often used to describe the spec-

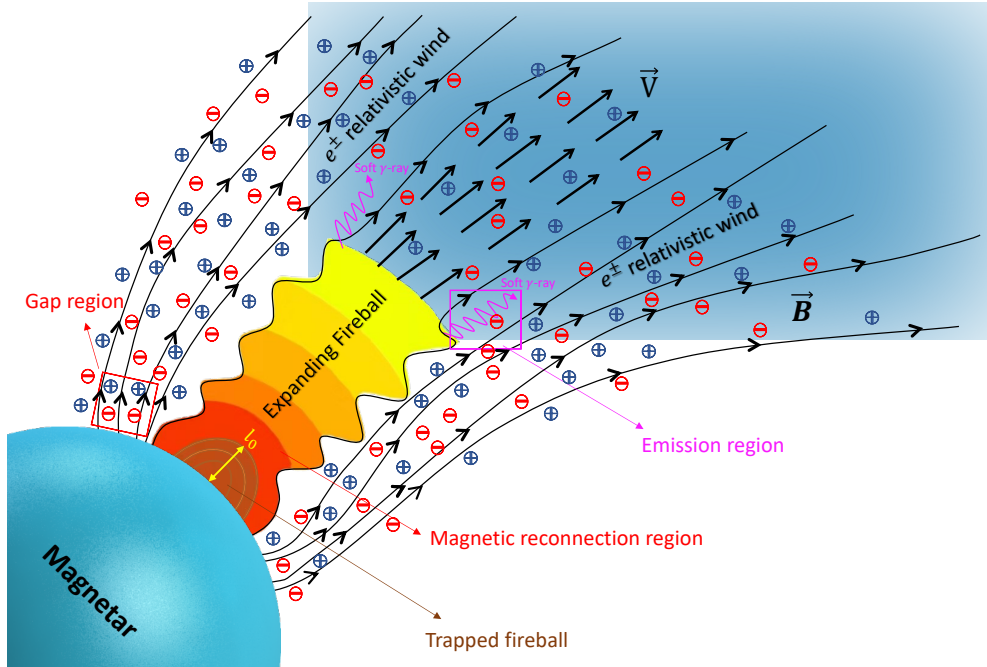


Figure 2. A schematic diagram of our model. A large number of high-energy photons accompanied by electron-positron pairs are released near the NS surface. A fraction of them is trapped in the confined magnetic field lines (dark red region). The other part breaks through the magnetic field lines due to sufficient radiation pressure and spreads out in the form of a relativistic expanding fireball along the magnetic tube. A large amount of dense e^\pm pairs (marked red and blue circle with \pm signs) are emitted from the gap region (red square), and accelerated by the gap potential difference. The pairs further propagate along the open field lines and form a wind zone at a larger radius (open blue region). The expanding fireball eventually penetrates the wind area, and the photons are scattered by the massive pairs in the emission region at photosphere radius (purple square), producing the high-energy γ -ray photons.

trum. However, since an extraordinarily high density of e^\pm pairs with a thermal distribution is supplied by the magnetar wind, an extra finite thermal medium (Compton cloud) emerges in the front of the expanding path of the fireball, which is highly opaque and leads to a series of radiation transfer effects including scatterings and absorption (Rybicki & Lightman 1986; Beloborodov 2010; Roberts et al. 2021). The occurrence of these energy transfer effects will change the spectral shape significantly. The photons, from either the thermal radiation of the fireball or the annihilation of e^\pm in the wind, are continuously scattered by a large number of e^\pm and finally escape at the photosphere in the form of thermal-like radiation through coherent scattering (CC) and inverse Compton (IC) scattering.

With a strong magnetic field and high number density of the pair plasma, photons with electric vector perpendicular to the magnetic field (E-mode) are easier to escape. The corresponding Rosseland mean optical depth (Duncan & Thomp-

son 1992; Meszaros & Rees 1992) of the fireball with a size of l is expressed as

$$\tau_\perp = \frac{4\pi^2}{5} \sigma_T \left(\frac{kT}{m_e c^2} \frac{B_Q}{B_R} \right)^2 n_{\perp l}, \quad (5)$$

where σ_T is the Thompson cross section, m_e is the electron mass, c is the light speed, and B_R is the magnetic field at radius R , i.e., $B_R = B_*(R/R_s)^{-3}$. By requiring $\tau_\perp = 1$, one can drive the minimal radiation radius of the expanding fireball as $l \sim 9 \times 10^5$ cm, which is about one order of magnitude larger than l_0 .

3. RADIATION AND FIT

Our model above predicts that the thermal photons of expanding fireball are subject to the coherent Compton scattering (CC) and incoherent Inverse Compton (IC) scattering, so the resulted spectrum is likely a modified blackbody (hereafter, MB¹) shape with an IC bump at

¹ We use “MB” to distinguish from multi-color blackbody (“MBB”; Meng et al. 2018, 2019, 2021; Wang et al. 2021).

the high-energy end. A parameterized function of the model-predicted spectrum can be derived by considering the above two radiation processes.

Whether the CC or IC dominates the radiation process are determined by the Compton y parameter, which varies at different photon energies. Following Rybicki & Lightman (1986), we define

$$y \equiv \frac{kT\bar{N}}{m_e c^2}, \quad (6)$$

where k is the Boltzmann constant, and \bar{N} is the mean scattering number when a photon travels a free path.

Depending on the y parameter, the derived flux can be considered in the following two regimes:

- For $y < 1$, CC dominates, and the energy of a scattered photon is not significantly changed. In this case, an MB spectral shape is expected. The specific intensity of CC is closely related to the scattering and absorption of the thermal photons (Rybicki & Lightman 1986):

$$I_{\nu}^{\text{CC}} = \frac{2B_{\nu}}{1 + \sqrt{(\kappa_{\text{ff}} + \kappa_{\text{es}})\kappa_{\text{ff}}^{-1}}}, \quad (7)$$

where κ_{ff} is the absorption factor of the free-free (bremsstrahlung) process in a thermal medium, κ_{es} is the scattering opacity from e^{\pm} plasma, and B_{ν} is the Planck function expressed as

$$B_{\nu} = \frac{2h\nu^3/c^2}{\exp(h\nu/kT) - 1}, \quad (8)$$

where h is the Planck constant. κ_{ff} and κ_{es} can be further written as

$$\kappa_{\text{es}} = \frac{\sigma_{\text{T}}}{m_e} = 730 \text{ cm}^2 \text{ g}^{-1}, \quad (9)$$

and

$$\begin{aligned} \kappa_{\text{ff}} &= \frac{4q_e^6}{3m_e hc} \left(\frac{2\pi}{3km_e} \right)^{1/2} T^{-1/2} n_{\pm}^2 \nu^{-3} \\ &\times (1 - e^{-x}) \bar{g}_{\text{ff}}(x) \\ &= 3.7 \times 10^8 T^{-1/2} n_{\pm}^2 \nu^{-3} (1 - e^{-x}) \bar{g}_{\text{ff}}(x), \end{aligned} \quad (10)$$

where q_e is the electron charge and $x \equiv h\nu/kT$. The $\bar{g}_{\text{ff}}(x)$ is the free-free Gaunt factor, and for the energy range in this study, it can be approximated as

$$\bar{g}_{\text{ff}}(x) \sim 3\pi^{-1/2} \ln(2.25/x). \quad (11)$$

Considering the Doppler boosting, the observed specific flux at a luminosity distance, D_{L} , can be calculated by

$$F_{\nu_{\text{obs}}}^{\text{CC}} = \frac{4\pi D^3}{c^2} \frac{h(\nu_{\text{obs}}/D)^3}{\exp\left(\frac{h\nu_{\text{obs}}}{DkT}\right) - 1} \left(1 + \sqrt{\frac{\kappa_{\text{ff}} + \kappa_{\text{es}}}{\kappa_{\text{ff}}}}\right)^{-1} \times \left(\frac{l_x}{D_{\text{L}}}\right)^2, \quad (12)$$

where D is the Doppler factor. $F_{\nu_{\text{obs}}}^{\text{CC}}$ strongly depends on the competition between κ_{ff} and κ_{es} , which can be easily noticed by introducing a characteristic frequency, $\nu_{0,\text{CC}}$, at which the scattering and absorption coefficients are equivalent, i.e.,

$$\kappa_{\text{es}} = \kappa_{\text{ff}}(\nu_{0,\text{CC}}). \quad (13)$$

For $\nu < \nu_{0,\text{CC}}$, absorption is more dominant, and Eq. (7) approaches the Rayleigh-Jeans limit and the observed spectrum (Eq. 12) is a pure blackbody. On the other hand, for $\nu > \nu_{0,\text{CC}}$, the scattering gradually becomes significant (see Figure 3) at higher energies and modifies the spectrum (Eq. 12) significantly.

For a pair plasma with a typical density of $n_{\pm} = 2.0 \times 10^{25} \text{ cm}^{-3}$ and temperature in range of 1-60 keV, it is calculated that $h\nu_{0,\text{CC}}$ is typically $\gtrsim 1.3 \text{ keV}$ in the comoving frame, as shown in Figure 3. Such a frequency falls well into the MeV range in the observer frame, confirming that the CC process is indeed necessary to be taken into account. This can also be verified by checking $x_{0,\text{CC}} \equiv h\nu_{0,\text{CC}}/kT \ll 1$, suggesting that photon at such a characteristic frequency is significantly subject to scattering in a hot plasma.

- For $y \gg 1$, the radiation is dominated by IC, and the energy is transferred from e^{\pm} pairs to the photons. In this case, the specific intensity can be approximated by the Wien law (Rybicki & Lightman 1986):

$$I_{\nu}^{\text{IC}} = \frac{2h\nu^3}{c^2} e^{-\alpha} e^{-x}, \quad (14)$$

where the factor $e^{-\alpha}$ is related to the local rate at which photons are produced, defined by (Landau & Lifshitz 1969)

$$e^{-\alpha} = \frac{N}{V} \left(\frac{h^2}{2\pi m k T} \right)^{3/2} \sim n_c \left(\frac{h^2}{2\pi m_c k T} \right)^{3/2}. \quad (15)$$

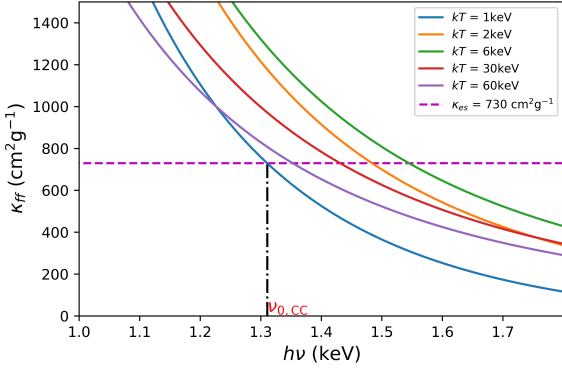


Figure 3. Absorption coefficient, κ_{eff} , as a function of photon energy at different equilibrium temperatures. The κ_{eff} evolves with the temperature, marked by the solid lines of different colors. The dashed line represents the κ_{es} . The dotted-dashed line marks the characteristic frequency $\nu_{0,CC}$ at $kT = 1 \text{ keV}$.

where m is the particle mass, N is the total number of particles, and V is the volume of the radiation region. n_c and m_c are defined as coupling number density and coupling mass, respectively. $e^{-\alpha}$ measures degeneracy of the particles. For example, $e^{-\alpha}$ is negligible if the particles meet the classical limit condition and are entirely non-degenerate. Otherwise, $e^{-\alpha}$ can be a significant number if the photons are coupling with the e^\pm pairs in a degenerate plasma.

The specific flux at the observer is

$$F_{\nu_{\text{obs}}}^{\text{IC}} = \frac{8\pi h\nu_{\text{obs}}^3}{c^2} e^{-\alpha} \exp\left(\frac{-h\nu_{\text{obs}}}{DkT}\right) \left(\frac{l_x}{D_L}\right)^2. \quad (16)$$

Another critical frequency, $\nu_{0,IC}$, is defined by requiring $y(\nu_{0,IC}) = 1$, above which IC process becomes significant. For pairs which follow the non-relativistic² thermal distributions in the comoving frame, $\nu_{0,IC}$ satisfies the relationship (Rybicki & Lightman 1986):

$$\kappa_{\text{es}} = \left(\frac{m_e c^2}{4kT}\right) \kappa_{\text{eff}}(\nu_{0,IC}). \quad (17)$$

Substituting Eq. (17) into Eq. (10), one can derive

² In the comoving frame, the mean Lorentz factor of the e^\pm pairs, $\langle\gamma_{\pm}\rangle$, can be estimated by $\langle\gamma_{\pm}\rangle = \sqrt{(12(kT/m_e c^2)^2)}$. For a characteristic temperature in our model, $T_c \sim 15 \text{ keV}$, $\langle\gamma_{\pm}\rangle \ll 1$.

$$x_{0,IC} \equiv \frac{h\nu_{0,IC}}{kT} \sim 2.4 \times 10^{17} (n_{\pm} m_e)^{1/2} T^{-9/4} \times [\bar{g}_{ff}(x_{0,IC})]^{1/2}. \quad (18)$$

From Eqs. (10), (13) and (17), we have

$$x_{0,IC} = \left(\frac{m_e c^2}{4kT}\right)^{1/2} x_{0,CC}. \quad (19)$$

The final observed flux can be calculated by combining Eqs. (12) and (16), i.e.,

$$F(\nu_{\text{obs}}, \Gamma, T, n_{\pm}, \alpha, l_0) = F_{\nu_{\text{obs}}}^{\text{MB}}(\Gamma, T, n_{\pm}, l_0) + F_{\nu_{\text{obs}}}^{\text{IC}}(\Gamma, T, \alpha, l_0), \quad (20)$$

which can be used to directly fit to the observed data. Note that we assumed an on-axis observer for Eq. (18) so the Doppler factor, $D = 1/[\Gamma(1 - \beta \cos\theta)]$, is replaced with the bulk Lorentz factor Γ of the pair plasma.

Considering the physical conditions, the priors and allowed ranges of the five free parameters in Eq. (20) are set up as follows:

- n_{\pm} : The number density of the e^\pm in the emission region. Log-uniformed distributed in range $[10^{24.5}, 10^{26.5}]$.
- T : The thermodynamic equilibrium temperature in the co-moving reference. kT is uniformed distributed in range $[5.0, 30.0]$.
- Γ : The bulk Lorentz factor of the pair plasma. Uniformed distributed in range $[35.0, 70.0]$.
- l_0 : The initial radius of the expanding fireball. Log-uniformed distributed in range $[10^{4.0}, 10^{6.0}]$.
- α : The index related to the IC intensity. Uniformed distributed in range $[0.0, 5.0]$ so $e^{-\alpha}$ is a significant number in range of $[0.007, 1]$.

We then collected the spectral data of GRB 200415A and performed the spectral analysis on the main burst region between 0.005 and 0.20 s, following the procedure of Yang et al. (2020). The data reduction follows the standard procedure described in (Zhang et al. 2011, 2016, 2018). Both time-integrated and time-dependent spectral analyses have been performed, between $T_0 - 0.005$ s and $T_0 + 0.20$ s. The spectral fitting slices are presented in Table 1. By employing the self-developed spectral fitting package, *McSpecfit* (Zhang

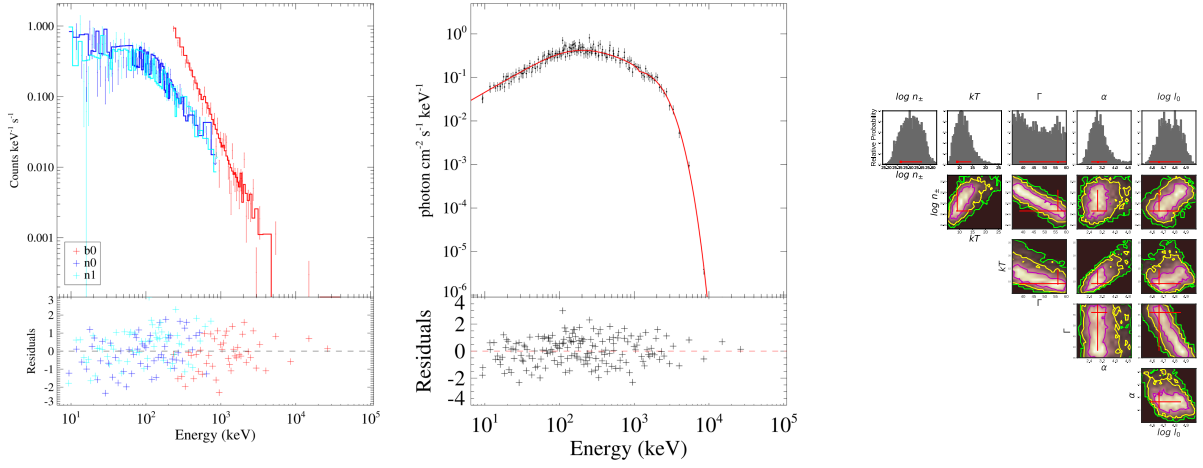


Figure 4. Time-integrated spectral fit of our model to the observed spectra of GRB 200415A between $T_0 - 0.005$ s and $T_0 + 0.20$ s. *Left:* observed photon count spectra over-plotted with best-fit model; *Middle:* Deconvolved model-predicated photon spectrum; *Right:* corner diagram of the parameter constraints. Histograms show the 1-D likelihood distribution of the fitting parameters, and contours show the 2-D likelihood map constrained by the MCMC method. Red crosses mark the best-fit values, and contours represent the 1-, 2-, 3- σ regions.

Table 1. The spectral fitting results of GRB 200415A

Time Interval (s)	Flux		Model Parameters						
	t_1	t_2	(erg cm $^{-2}$ s $^{-1}$)	$\log_{10}(n_{\pm}/\text{cm}^{-3})$	kT (keV)	Γ	α	$\log_{10}(l_0/\text{cm})$	PGSTAT/dof
-0.005	0.20	$2.30^{+0.83}_{-0.48} \times 10^{-3}$	$25.40^{+0.29}_{-0.005}$	$9.17^{+5.41}_{-0.48}$	$56.09^{+3.90}_{-17.86}$	$2.91^{+0.60}_{-0.40}$	$4.66^{+0.19}_{-0.09}$	290.17/349	
-0.005	-0.001	$0.01^{+0.01}_{-0.01}$	$25.40^{+0.24}_{-0.13}$	$6.11^{+5.54}_{-0.12}$	$52.21^{+8.08}_{-14.02}$	$2.51^{+1.62}_{-0.17}$	$5.61^{+0.13}_{-0.14}$	253.4/349	
-0.001	0.01	$0.02^{+0.01}_{-0.01}$	$26.04^{+0.15}_{-0.09}$	$15.07^{+0.42}_{-0.02}$	$55.09^{+1.80}_{-0.10}$	$1.99^{+0.04}_{-0.10}$	$4.87^{+0.04}_{-0.05}$	284.8/349	
0.01	0.04	$3.97^{+1.70}_{-0.92} \times 10^{-3}$	$25.99^{+0.42}_{-0.41}$	$12.60^{+8.24}_{-0.51}$	$67.80^{+2.16}_{-27.45}$	$4.99^{+0.01}_{-0.98}$	$4.65^{+0.29}_{-0.05}$	245.9/349	
0.04	0.12	$8.58^{+5.57}_{-1.98} \times 10^{-4}$	$25.70^{+0.37}_{-0.02}$	$5.06^{+7.90}_{-0.06}$	$49.53^{+11.68}_{-10.65}$	$1.12^{+3.48}_{-0.12}$	$5.12^{+0.04}_{-0.09}$	237.5/349	
0.012	0.20	$1.41^{+12.74}_{-0.59} \times 10^{-5}$	$25.81^{+0.45}_{-0.67}$	$5.10^{+6.06}_{-0.10}$	$35.62^{+17.23}_{-0.62}$	$4.43^{+0.32}_{-1.26}$	$4.93^{+0.16}_{-0.52}$	178.1/349	

et al. 2018), we were able to fit the spectral data using our model in Eq. (20). The time-integrated fit fit is shown in Figure 4. The best-fit parameters, along with the corresponding energy flux in each slice, are listed in Table 1.

The values of the goodness of fit (PGSTAT/dof) in Table 1 indicate that our model successfully explains the observation. The values of best-fit parameters are overall consistent with the theoretical predictions as highlighted below:

- n_{\pm} is constrained to a relatively stable value between 10^{25} - 10^{26} cm $^{-3}$, which is well consistent with the estimation in Eq. (3).

- kT clearly shows an intensity tracking pattern with a peak value at $kT = 15.7^{+0.42}_{-0.02}$ keV.

- Γ is constrained within the range of $\sim [50, 68]$, much smaller than those in GRBs. Our results are also consistent with the lower limit (i.e., $\Gamma > 6$) given by Roberts et al. (2021).

- l_0 is stably constrained at $\sim 10^5$ cm, which is consistent with model estimation in Eq. (2).

In Figure 5, we plot the best-fit values of the n_{\pm} and kT along the critical lines defined by $\kappa_{\text{ff}}(n_{\pm}, kT, \nu) = \kappa_{\text{es}}$, above which scattering becomes dominated. Our results suggest a lower limit of the photon energy for the scattering to take dominated effect (thus the modified black-body component can emerge), which roughly is > 1 keV in the comoving frame, or > 50 keV in the observer frame by multiplying the Γ values in Table 1.

4. SUMMARY

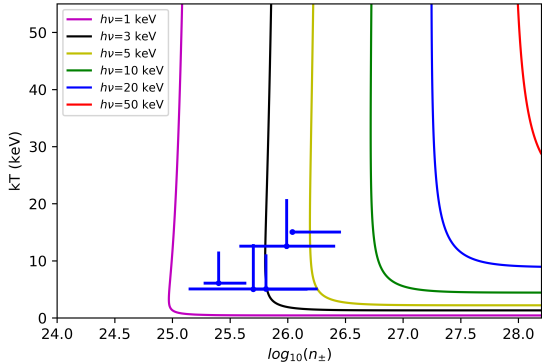


Figure 5. The equivalent lines of $\kappa_{ff} = \kappa_{es}$ for different photon energies in the n_{\pm} - kT parameter space. The region above each line indicates where scattering becomes dominant. Constraints from our spectral fitting of the observed data are marked with blue dots.

In this *Letter*, we introduced a physical model which involves a fireball bubble emerging from the magnetar surface due to violent neutron star activities such as crust cracking or magnetic reconnection. We studied in detail the evolution of such a fireball, including its expansion and interaction with the magnetar e^{\pm} wind. We found that high-energy photons at the photosphere radius are Comptonized by the high-number-density e^{\pm} relativistic wind, which results in a modified blackbody spectrum with a Wien tail. Through a direct Monte-Carlo fit, our physical model is found well consistent with the observed spectra of GRB 200415A. Our results, for the first time, confirm the physical origin of the magnetar giant flares through first-principle theoretical calculations as well as the evidence of data consistency.

ACKNOWLEDGMENTS

We thank Di Xiao, Ken Chen, Qiao-Chu Li, Ze-Nan Liu, Jun Yang for helpful discussions and constructive comments. Z.J.Z. appreciates the help from Tianyue Li (School of Physics, NJU) and Shan Xiang (GXU) for their illustration support. We acknowledge the use of public data from the Fermi Science Support Center (FSSC). B.B.Z acknowledges support by Fundamental Research Funds for the Central Universities (14380046), the National Key Research and Development Programs of China (2018YFA0404204), the National Natural Science Foundation of China (Grant Nos. 11833003, U2038105), the science research grants from the China Manned Space Project with NO.CMS-CSST-2021-B11, and the Program for Innovative Talents, Entrepreneur in Jiangsu. Y.Z.M. is supported by the National Postdoctoral Program for Innovative Talents (grant No. BX20200164).

REFERENCES

- Atteia, J. L., Boer, M., Hurley, K., et al. 1987, *ApJL*, 320, L105, doi: [10.1086/184984](https://doi.org/10.1086/184984)
- Beloborodov, A. M. 2010, *MNRAS*, 407, 1033, doi: [10.1111/j.1365-2966.2010.16770.x](https://doi.org/10.1111/j.1365-2966.2010.16770.x)
- Bissaldi, E., Briggs, M., Burns, E., et al. 2020, GRB Coordinates Network, 27587, 1
- Boggs, S. E., Zoglauer, A., Bellm, E., et al. 2007, *The Astrophysical Journal*, 661, 458, doi: [10.1086/516732](https://doi.org/10.1086/516732)
- Duncan, R. C., & Thompson, C. 1992, *ApJL*, 392, L9, doi: [10.1086/186413](https://doi.org/10.1086/186413)
- Feroci, M., Hurley, K., Duncan, R. C., & Thompson, C. 2002, *Mem. Soc. Astron. Italiana*, 73, 554
- Golenetskii, S. V., Ilinskii, V. N., & Mazets, E. P. 1984, *Nature*, 307, 41, doi: [10.1038/307041a0](https://doi.org/10.1038/307041a0)
- Gourgouliatos, K. N., Wood, T. S., & Hollerbach, R. 2016, *Proceedings of the National Academy of Science*, 113, 3944, doi: [10.1073/pnas.1522363113](https://doi.org/10.1073/pnas.1522363113)
- Hurley, K., Cline, T., Mazets, E., et al. 1999, *Nature*, 397, 41, doi: [10.1038/16199](https://doi.org/10.1038/16199)
- Israel, G. L., Belloni, T., Stella, L., et al. 2005, *ApJL*, 628, L53, doi: [10.1086/432615](https://doi.org/10.1086/432615)
- Israel, G. L., Esposito, P., Rea, N., et al. 2016, *MNRAS*, 457, 3448, doi: [10.1093/mnras/stw008](https://doi.org/10.1093/mnras/stw008)
- Kaspi, V. M., & Beloborodov, A. M. 2017, *ARA&A*, 55, 261, doi: [10.1146/annurev-astro-081915-023329](https://doi.org/10.1146/annurev-astro-081915-023329)
- Katz, J. I. 2020, *MNRAS*, 499, 2319, doi: [10.1093/mnras/staa3042](https://doi.org/10.1093/mnras/staa3042)
- Kumar, P., & Bošnjak, Ž. 2020, *MNRAS*, 494, 2385, doi: [10.1093/mnras/staa774](https://doi.org/10.1093/mnras/staa774)
- Landau, L. D., & Lifshitz, E. M. 1969, *Statistical physics*. Pt.1
- Laros, J. G., Fenimore, E. E., Fikani, M. M., Klebesadel, R. W., & Barat, C. 1986, *Nature*, 322, 152, doi: [10.1038/322152a0](https://doi.org/10.1038/322152a0)
- Lin, L., Zhang, C. F., Wang, P., et al. 2020, *Nature*, 587, 63, doi: [10.1038/s41586-020-2839-y](https://doi.org/10.1038/s41586-020-2839-y)
- Mazets, E. P., Golenetskij, S. V., & Guryan, Y. A. 1979a, *Soviet Astronomy Letters*, 5, 343
- Mazets, E. P., Golentskii, S. V., Ilinskii, V. N., Aptekar, R. L., & Guryan, I. A. 1979b, *Nature*, 282, 587, doi: [10.1038/282587a0](https://doi.org/10.1038/282587a0)
- Meng, Y.-Z., Geng, J.-J., Zhang, B.-B., et al. 2018, *ApJ*, 860, 72. doi: [10.3847/1538-4357/aac2d9](https://doi.org/10.3847/1538-4357/aac2d9)
- Meng, Y.-Z., Liu, L.-D., Wei, J.-J., et al. 2019, *ApJ*, 882, 26. doi: [10.3847/1538-4357/ab30c7](https://doi.org/10.3847/1538-4357/ab30c7)
- Meng, Y.-Z., Geng, J.-J., & Wu, X.-F. 2021, arXiv:2107.04532
- Mereghetti, S. 2008, *A&A Rv*, 15, 225, doi: [10.1007/s00159-008-0011-z](https://doi.org/10.1007/s00159-008-0011-z)
- Mereghetti, S., Pons, J. A., & Melatos, A. 2015, *SSRv*, 191, 315, doi: [10.1007/s11214-015-0146-y](https://doi.org/10.1007/s11214-015-0146-y)
- Meszaros, P., & Rees, M. J. 1992, *MNRAS*, 257, 29P, doi: [10.1093/mnras/257.1.29P](https://doi.org/10.1093/mnras/257.1.29P)
- Metzger, B. D., Margalit, B., & Sironi, L. 2019, *MNRAS*, 485, 4091. doi: [10.1093/mnras/stz700](https://doi.org/10.1093/mnras/stz700)
- Moffatt, H. K. 1985, *Journal of Fluid Mechanics*, 159, 359, doi: [10.1017/S0022112085003251](https://doi.org/10.1017/S0022112085003251)
- Parker, E. N. 1983a, *ApJ*, 264, 635, doi: [10.1086/160636](https://doi.org/10.1086/160636)
- . 1983b, *ApJ*, 264, 642, doi: [10.1086/160637](https://doi.org/10.1086/160637)
- Roberts, O. J., Veres, P., Baring, M. G., et al. 2021, *Nature*, 589, 207, doi: [10.1038/s41586-020-03077-8](https://doi.org/10.1038/s41586-020-03077-8)
- Ruderman, M. A., & Sutherland, P. G. 1975, *ApJ*, 196, 51, doi: [10.1086/153393](https://doi.org/10.1086/153393)
- Rybicki, G. B., & Lightman, A. P. 1986, *Radiative Processes in Astrophysics*
- Strohmayer, T. E., & Watts, A. L. 2005, *ApJL*, 632, L111, doi: [10.1086/497911](https://doi.org/10.1086/497911)
- Svinkin, D., Frederiks, D., Hurley, K., et al. 2021, *Nature*, 589, 211, doi: [10.1038/s41586-020-03076-9](https://doi.org/10.1038/s41586-020-03076-9)
- Thompson, C., & Duncan, R. C. 1995, *MNRAS*, 275, 255, doi: [10.1093/mnras/275.2.255](https://doi.org/10.1093/mnras/275.2.255)
- . 2001, *ApJ*, 561, 980, doi: [10.1086/323256](https://doi.org/10.1086/323256)
- Wang, X. I., Zheng, X., Xiao, S., et al. 2021, arXiv:2107.10452
- Yamazaki, R., Ioka, K., Takahara, F., & Shibasaki, N. 2006, in *Journal of Physics Conference Series*, Vol. 31, *Journal of Physics Conference Series*, 99–102, doi: [10.1088/1742-6596/31/1/016](https://doi.org/10.1088/1742-6596/31/1/016)
- Yang, J., Chand, V., Zhang, B.-B., et al. 2020, *ApJ*, 899, 106, doi: [10.3847/1538-4357/aba745](https://doi.org/10.3847/1538-4357/aba745)
- Yang, Y.-P., & Zhang, B. 2015, *ApJ*, 815, 45, doi: [10.1088/0004-637X/815/1/45](https://doi.org/10.1088/0004-637X/815/1/45)
- Zhang, B.-B., Uhm, Z. L., Connaughton, V., Briggs, M. S., & Zhang, B. 2016, *ApJ*, 816, 72, doi: [10.3847/0004-637X/816/2/72](https://doi.org/10.3847/0004-637X/816/2/72)
- Zhang, B.-B., Zhang, B., Liang, E.-W., et al. 2011, *ApJ*, 730, 141, doi: [10.1088/0004-637X/730/2/141](https://doi.org/10.1088/0004-637X/730/2/141)
- Zhang, B. B., Zhang, B., Castro-Tirado, A. J., et al. 2018, *Nature Astronomy*, 2, 69, doi: [10.1038/s41550-017-0309-8](https://doi.org/10.1038/s41550-017-0309-8)
- Zhang, B. 2020, *Nature*, 587, 45, doi: [10.1038/s41586-020-2828-8](https://doi.org/10.1038/s41586-020-2828-8)